ELSEVIER

Chemistry & Biology 8 (2001) 1253–1264

Chemistry & Biology

www.elsevier.com/locate/chembiol

Research Paper

# Structure of cephalosporin acylase in complex with glutaryl-7-aminocephalosporanic acid and glutarate: insight into the basis of its substrate specificity

Youngsoo Kim [a,b,*], Wim G.J. Hol [b,c]

[a] *School of Chemical Engineering, Yeungnam University, Dae-Dong, Kyungsan 712-749, South Korea*

[b] *Departments of Biological Structure and Biochemistry, Biomolecular Structure Center, University of Washington, P.O. Box 357742, Seattle, WA 98195-7742, USA*

[c] *Howard Hughes Medical Institute, University of Washington, P.O. Box 357742, Seattle, WA 98195-7742, USA*

Received 4 July 2001; revisions requested 30 August 2001; revisions received 21 September 2001; accepted 28 September 2001
First published online 7 November 2001

**Abstract**

**Background:** Semisynthetic cephalosporins are primarily synthesized from 7-aminocephalosporanic acid (7-ACA), which is obtained by environmentally toxic chemical deacylation of cephalosporin C (CPC). Thus, the enzymatic conversion of CPC to 7-ACA by cephalosporin acylase (CA) would be of great interest. However, CAs use glutaryl-7-ACA (GL-7-ACA) as a primary substrate and the enzyme has low turnover rates for CPC.

**Results:** The binary complex structures of CA with GL-7-ACA and glutarate (the side-chain of GL-7-ACA) show extensive interactions between the glutaryl moiety of GL-7-ACA and the seven residues that form the side-chain pocket. These interactions explain why the D-α-aminoadipyl side-chain of CPC yields a poorer substrate than GL-7-ACA.

**Conclusions:** This understanding of the nature of substrate specificity may be useful in the design of an enzyme with an improved performance for the conversion of CPC to 7-ACA. Additionally, the catalytic mechanism of the deacylation reaction was revealed by the ligand bound structures. 

**Keywords:** Cephalosporin acylase; Glutaryl-7-aminocephalosporanic acid; Cephalosporin antibiotic; Substrate specificity

## 1. Introduction

Semisynthetic cephalosporins are the most widely used antibiotics. Cephalosporin C (CPC), the natural form of cephalosporin, is produced as a secondary metabolite by the fungus *Cephalosporium acremonium* (chemical formulas of related compounds in Fig. 1a). The total worldwide market value for cephalosporin antibiotics ranks fifth among the leading therapeutic agents worldwide [1]. All clinically important semisynthetic derivatives of cephalosporins are manufactured from 7-aminocephalosporanic acid (7-ACA) or 7-aminodeacetoxycephalosporanic acid (7-ADCA). 7-ACA, a starting compound for the industrial production of semisynthetic cephalosporins, can be obtained by chemical deacylation of CPC using toxic compounds, such as iminoether, nitrosyl chloride, and methanol [2]. This chemical method includes several expensive chemical steps and requires a thorough treatment of the toxic chemical waste in order to overcome environmental safety problems. Because of the environmental interest, the pharmaceutical industry needs to look into the possibility of using the enzymatic process. Currently, a 3-step/2-enzyme enzymatic process [3] is being utilized in a few European companies, such as Hoechst and Antibioticos, but the majority of 7-ACA is still produced by the chemical process (personal communication, Amicogen Company, South Korea). 7-ADCA, the other starting compound for semisynthetic cephalosporins, is also produced by an expensive multistep and chemical ring expansion of penicillin G, followed by enzymatic deacylation using penicillin

*Abbreviations:* 7-ACA, 7-aminocephalosporanic acid; CPC, cephalosporin C; GL-7-ACA, glutaryl-7-ACA; 7-ADCA, 7-aminodeacetoxycephalosporanic acid; GL-7-ADCA, glutaryl-7-ADCA; Ntn, N-terminal; CA, cephalosporin acylase; CAD, a class I CA from *Pseudomonas diminuta* KAC-1; CA16, a CA from *Pseudomonas* sp. GK16; PGA, penicillin G acylase; DTT, dithiothreitol; PEG, polyethylene glycol; APS, Advanced Photon Source; PMSF, phenylmethylsulfonyl fluoride

* Corresponding author.
*E-mail address:* ykim1@yu.ac.kr (Y. Kim).

1074-5521/01/$ – see front matter 
PII: S1074-5521(01)00092-8

G acylase (PGA) [4]. A recent report proposed that recombinant strains of *Acremonium chrysogenum* might produce deacetoxy CPC by fermentation, which can be subsequently converted to 7-ADCA using enzymatic conversion by cephalosporin acylase (CA) [5]. This is an interesting approach, even though it would probably take a significant effort to commercialize the process of producing deacetoxy CPC from the recombinant fungus, *A. chrysogenum*. Clearly, an enzymatic conversion of CPC to 7-ACA, and of deacetoxy CPC to 7-ADCA, is of great interest in the manufacture of cephalosporin antibiotics [6,7]. However, the biggest problem in enzymatic production appears to be that CA takes glutaryl-7-ACA (GL-7-ACA) or glutaryl-7-ADCA as a primary substrate (GL-7-ADCA). Also, its substrate specificity for CPC or deacetoxy CPC is too low to be applicable for industrial production of 7-ACA or 7-ADCA [8–12]. Unsuccessful attempts to obtain a direct enzymatic transformation of CPC into 7-ACA by a single CA led to the development of the 3-step/2-enzyme process, which is the furthest along in developing a way to replace the toxic chemical process with an enzymatic process [3]. However, this 3-step/2-enzyme process does not provide a marked economical advantage over the chemical process for the pharmaceutical industry [3,13].

CAs have been categorized into five classes (CA I–V) [14]. They are able to catalyze several substrates and substrate analogs, but their activities on CPC vary from 0–4% relative to GL-7-ACA [12]. Much effort has been devoted to screening CAs from soil strains, which can convert CPC into 7-ACA by a single enzymatic conversion. However, this effort has been unsuccessful in obtaining a CA that carries high activity with respect to CPC [8,10]. As well, the site-directed mutagenesis technique for a known CA has been employed in order to improve the activity with respect to CPC. However, this effort only improved the activity for CPC by less than 2-fold compared to the wild enzyme [9,11]. The absence of a three-dimensional structure of any CA has been a handicap for these protein-engineering studies.

We recently solved the first CA structure at 2.0 Å resolution [12]. This CA is a class I enzyme from *Pseudomonas diminuta* KAC-1. It is abbreviated hereafter as CAD. CAD shows acylase activity for GL-7-ACA and GL-7-ADCA, but it can not efficiently use CPC, penicillin G, or ampicillin as substrates [15,16]. The CAD structure appeared to be a single domain heterodimer that consists of a α-subunit and a β-subunit [12]. The structure of this enzyme is of interest, not only for understanding its substrate specificity, but also in providing structural evidence that the four different classes of CAs (classes I–IV) can be grouped into one family of the N-terminal (Ntn) hydrolase superfamily [12,17]. The CAD structure provides a structural basis for the protein-engineering studies that are aimed at improving the activity of various classes of CAs (classes I–IV) with respect to CPC [12].

In this report, we extended our structural work on CAD. Two structures of the binary complexes of CAD with GL-7-ACA (the most favored substrate of CAs) and glutarate (the side-chain of GL-7-ACA that determines the substrate specificity of GL-7-ACA), were solved at the 2.6 and 2.5 Å resolutions, respectively. The observed interactions between ligands and active-site residues reveal why GL-7-ACA is the most favored substrate of a CA, and conversely why CPC is not a good substrate for a CA. We also discuss how one could modify the active site of CAs to improve in activity with respect to CPC. Finally, a catalytic mechanism for the deacylation reaction can be proposed based on two ligand bound structures.

## 2. Results and discussion

### 2.1. Structures of complexes

The structures of the two binary complexes of CAD, one with GL-7-ACA and the other with glutarate, were determined. The X-ray diffraction and refinement statistics data are summarized in Table 1. In the course of these two structure determinations, the $F_o-F_c$ difference Fourier maps showed positive densities for the ligands (Fig. 1b–d), clearly defining the shapes of GL-7-ACA and glutarate prior to adding information of these ligands to the coordinate sets. The structures of GL-7-ACA and glutarate were built into the densities using XtalView/Xfit [18] and O [19]. The structures of cephalosporin antibiotics, such as cephalothin and cefotaxime, are available from the Cambridge Structural Database. Their refined structures containing a four-membered β-lactam ring fused to a six-membered ring, were previously reported [20–22]. The refined structure of GL-7-ACA keeps a similar conformational shape for the two rings [20–22]. However, the angles that are generated by the two fused rings in GL-7-ACA are optimized to the diffraction data by the simulated annealing of CNS [23], as shown in Fig. 1b. The initial model of the glutarate:CAD complex was easily built, using the defined $F_o-F_c$ difference Fourier map (Fig. 1d) and the refinement was straightforward.

There is only a minor difference in the crystallization conditions between the apo and complex structures of CAD. The apo-CAD crystal was grown at pH 6.5 [12], while complex CAD crystals were obtained at pH 5.5. However, the crystal structures of the two binary complexes lost 0.5 Å resolution compared to apo-CAD, whose structure was determined to 2.0 Å resolution. Several attempts to determine the binding mode of the two ligands to CAD by soaking apo-crystals in a solution of GL-7-ACA and glutarate resulted in no density for the ligands. Once suitable co-crystals of CAD:GL-7-ACA and CAD:glutarate complexes were obtained, soaking experiments were no longer pursued.

There are four known class I CAs: CAs from *Pseudo-*

Table 1
Summary of crystallographic data

| | GL-7ACA | Glutarate |
|---|---|---|
| Diffraction data statistics | | |
| Space group | $P4_12_12$ | $P4_12_12$ |
| Unit cell dimensions (Å) | $a=b=74.1$, $c=379.8$ | $a=b=73.7$, $c=381.2$ |
| Wavelength (Å) | 1.03320 | 1.06296 |
| Resolution range[a] (Å) | 20–2.6 (2.69–2.60) | 20–2.5 (2.59–2.50) |
| Completeness (%) | 98.3 (92.1) | 98.1 (95.0) |
| Reflections, total | 196351 | 156206 |
| Reflections, unique | 32457 | 36332 |
| $R_{sym}$ (%)[b] | 6.0 (58.7) | 7.5 (47.8) |
| $I/\sigma$ | 22.9 (1.98) | 17.9 (2.42) |
| X-ray source | SBC-CAT (APS) | SBC-CAT (APS) |
| Refinement statistics | | |
| Resolution (Å) | 20–2.6 | 20–2.5 |
| $R^c_{cryst}$ | 19.0 | 18.8 |
| $R^d_{free}$ | 21.3 | 23.0 |
| Number of non-H atoms | | |
| protein | 5299 | 5299 |
| water | 416 | 416 |
| ligand | 26 | 9 |
| r.m.s. deviation | | |
| bonds (Å) | 0.0060 | 0.0055 |
| angles (°) | 1.27 | 1.29 |
| Average *B*-factors | 45.0 | 30.8 |

[a] Values within parenthesis are for the last shell of data.
[b] $R_{sym} = |I-\langle I\rangle|/I$.
[c] $R_{cryst} = \||F_{obs}|-|F_{calc}\|/|F_{obs}|$. All data were used with no $\sigma$ cutoff.
[d] $R_{free} = ||F_{obs}|-|F_{calc}||/|F_{obs}|$, where $F_{obs}$ are test set amplitudes (3.5%), not used in refinement. All data were used with no $\sigma$ cutoff.

*monas* sp. GK16, *Pseudomonas* sp. 130, *Pseudomonas* sp. C427, and *P. diminuta* KAC-1 [7,12,14]. Amino acid sequences of all Class I CAs are at least 97% identical to one another in the well characterized regions [12]. In particular, the amino acid sequence of the α-chain of a CA from *Pseudomonas* sp. GK16 (CA16) is identical to CAD. Only one amino acid of the β-chain (Thr112β) is different from CAD (Ser112β), however, the amino acid sequence of the β chain in CA16 was reported only for residues from 1 to 113 [7]. Kinetic parameters are well characterized for CA16 [24]. These parameters may provide an overall insight into the kinetic behavior for CAD because CAD and CA16 can be considered as practically identical enzymes in view of their high degree of amino acid identities. The pH dependence of steady-state kinetics and the kinetic parameters for CA16 were reported previously (31). $K_m$ and $k_{cat}$ are 1.05 mM and 9.48 $s^{-1}$ at pH 7.0 respectively, and $k_{cat}/K_m$ reaches a maximum at pH 8.0 (about 9 $s^{-1}$ $mM^{-1}$). The $k_{cat}/K_m$ value at pH 5.5 dropped to about 2.5, which corresponds to 28% of the maximum value at pH 8.0. The co-crystallization of CAD with GL-7-ACA was carried out at pH 5.5 and co-crystals were grown overnight. The low pH most likely contributes to the decreased deacylation activity so that intact GL-7-ACA remains bound to active CAD during crystal growth. The $F_o-F_c$ difference electron density in the active site (Fig. 1b,c) of the CAD crystals, grown in the presence of GL-7-ACA, matches well with the intact GL-7-ACA, but some electron density is deficient around the C7 of the β-lactam ring. This reflects the fact that CAD is still active in the crystalline state at pH 5.5, thus an average density of the enzyme in complex with substrate and products is obtained.

### *2.2. Interactions between CAD and ligands*

The active site can be divided into three binding sites for each of the three components of a substrate like GL-7-ACA: (1) the side-chain site, in this case the glutaryl moiety ($R_1$ of ligand I in Fig. 1a) that is attached to C7 of the β-lactam ring of the substrate, (2) the 4-membered β-lactam that is fused to a six-membered ring (two fused rings in ligand I in Fig. 1a), (3) binding sites for two branched chains attached to the six-membered ring of ligand. In Fig. 1a, these are the carboxylate and an acetoxymethyl moiety ($R_2$ in the figure). In both binary complexes the glutaryl side-chain is buried inside a deep pocket (Fig. 2A,B).

The most extensive interactions between the protein and GL-7-ACA involve the glutaryl side-chain of GL-7-ACA. Three residues in the side-chain pocket (Arg57β, Tyr149α, and Tyr33β) make tight hydrogen bonds with this critical part of the substrate. Arg57β is a key player in binding this side-chain moiety with the two side-chain atoms, NH1 and NH2, thus making two hydrogen bonds with the O2 of the negatively charged carboxylate group (Fig. 2C). In addition, the same oxygen atom of this carboxylate group is held in place by another hydrogen bond with the side-

a

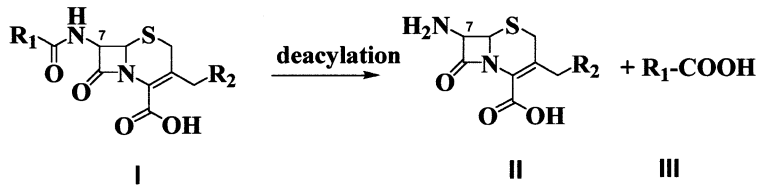


I II III

| Ligand I[1] | $R_1$ | $R_2$ |
|---|---|---|
| CPC | -$(CH_2)_3$-$CH(NH_2)$-COOH | -$OCOCH_3$ |
| Deacetoxy CPC | -$(CH_2)_3$-$CH(NH_2)$-COOH | -H |
| GL-7-ACA | -$(CH_2)_3$-COOH | -$OCOCH_3$ |
| GL-7-ADCA | -$(CH_2)_3$-COOH | -H |
| **Ligand II** | **$R_1$** | **$R_2$** |
| 7-ACA | - | -$OCOCH_3$ |
| 7-ADCA | - | -H |

| Ligand III | |
|---|---|
| Glutarate | HOOC-$(CH_2)_3$-COOH |
| D-α-aminoadipate | HCOO-$(CH_2)_3$-$CH(NH_2)$-COOH |

[1] Number I, II, II under the chemical formulas stand for the ligands I, II, III.

Fig. 1. Chemical formulas of ligands, and stereoview of $F_o-F_c$ difference Fourier maps. (a) Chemical formulas of compounds involved in the deacylation reaction by CA. (b) $F_o-F_c$ difference Fourier map of GL-7-ACA, (c) $F_o-F_c$ difference Fourier map of GL-7-ACA rotated by 120° versus (b). (d) $F_o-F_c$ difference Fourier map of glutarate. Coefficients for difference Fourier maps are $|F_{obs,\ complex}|-|F_{calc,\ model\ with\ ligands\ omitted}|$, using $\Phi_{calc,\ with\ ligand\ omitted}$. The maps are contoured at 2.5 $\sigma$ and atoms that will be discussed are labeled.

chain OH of Tyr33β. The other oxygen atom of the carboxylate group, O1, is hydrogen-bonded to the phenol hydroxyl of Tyr149α. Gln50β, which may be involved in substrate binding [12], does not make direct hydrogen bonds with the glutarate moiety of GL-7-ACA (Fig. 2C). However, it may still play a significant role in substrate binding, since its side-chain atoms, OE1 and NE2, make hydrogen bonds with the side-chain NH1 of the critical Arg57β and with the OH of Tyr149α, respectively. These two hydrogen bonds may direct the side-chains of Arg57β and Tyr149α to the proper position for it to interact with the substrate in the side-chain pocket (Fig. 2C).

In addition to the hydrogen bonds of the carboxylate group, four carbon atoms of the glutaryl moiety are stabilized by hydrophobic interactions with neighboring hydrophobic residues. Atoms C15, C17, C5, and C9 of the glutarate moiety are engaged in hydrophobic interactions with atoms CD2 of Leu24β, CD2 of Leu24β, CB of Val70β, and CE2 of Phe177β, respectively. The binding mode of the glutaryl moiety of GL-7-ACA (Fig. 2C) is such that every atom of the carboxylate group, except the C11 carbon atom, is interacting with active-site residues by either the hydrogen bond or hydrophobic interactions. These precise individual interactions of the glutarate moiety of GL-7-ACA with the residues forming the side-chain pocket contribute to the specificity of CA for GL-7-ACA.

Interestingly, the two fused rings of GL-7-ACA form no hydrophilic interaction with active-site residues, but these two rings are engaged in four hydrophobic interactions: the S1, C2, C6, and C8 atoms contact side-chain atoms CE2 and CD2 of Tyr149α, CG2 of Val70β, and CD2 of Leu24β, respectively (Fig. 2A,C). On the other hand, only one branched chain from the six-membered ring (the acetoxymethyl group, $R_2$ of ligand I in Fig. 1a) makes hydrophobic and hydrogen bonding interactions with the enzyme. The carbonyl oxygen, O3, of the acetoxymethyl group forms two hydrogen bonds with side-chain atoms NH1 and NH2 of Arg155α that are located at the opposite side of the Arg57β in the side-chain binding pocket. In addition, the carbon atoms C13 and C14 of the acetoxy group form hydrophobic interactions with the side-chain CB of Ser152α. Also, the carbon atom C13 makes another hydrophobic interaction with the side-chain atom CZ of Arg155α (Fig. 2C). In contrast, the other branched chain of the six-membered ring (the carboxylate group) is exposed to solvent. It makes a hydrogen bond with a water molecule, but makes no interactions with the protein.

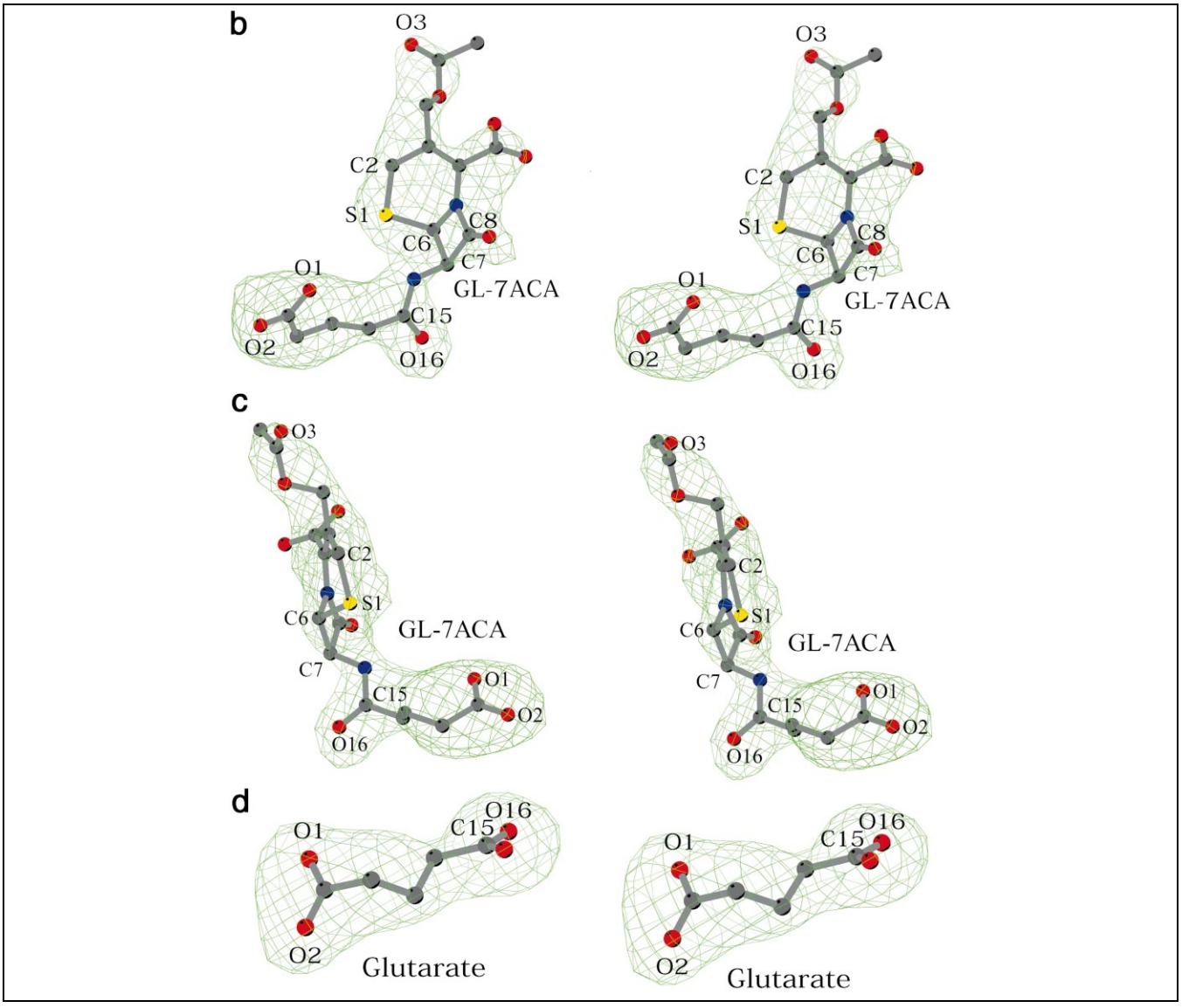


Fig. 1 (*Continued*).

It is clear that the two important arginines in the active site, Arg57β and Arg155α, play a key role in substrate recognition by anchoring the two opposite ends ($R_1$ and $R_2$ of ligand I in Fig. 1a) of the substrate. The intensive interactions of the side-chain of GL-7-ACA explain why different side-chains of potential CA substrates have a great influence on enzyme activity. For example, changing the glutaryl side-chain of GL-7-ACA into a D-α-amino-adipyl moiety, which is the side-chain of CPC, dramatically reduces the activity in all CAs, even though all of the other parts of both substrates are the same.

### 2.3. *Involvement of the fused rings of substrate in deacylation reaction*

Penicillins carry a four-membered β-lactam ring fused to a five-membered ring as a backbone whereas cephalosporins bear a four-membered β-lactam ring fused to a six-membered ring. It has been proposed that in penicillin acylase the four-membered β-lactam ring is unnecessary for the deacylation reaction. Penicillin acylases can also react with substrates lacking the two fused rings [25,26]. In addition, it has been proposed [12] that the two fused rings may not be engaged in extensive specific interactions with active-site residues of CA, because the active-site conformation is similar to PGA and so CA probably has substrate binding modes and a catalytic pathway analogous to those of PGA [27,28]. However, this proposal [25,26] should be corrected for presenting reference in view of the observation that the β-lactam ring fused to the six-membered ring is engaged in several specific hydrophobic interactions with the enzyme in the GL-7-ACA bound structure of CAD (Fig. 3C). Likely, these hydrophobic interactions are not a critical factor in recognizing

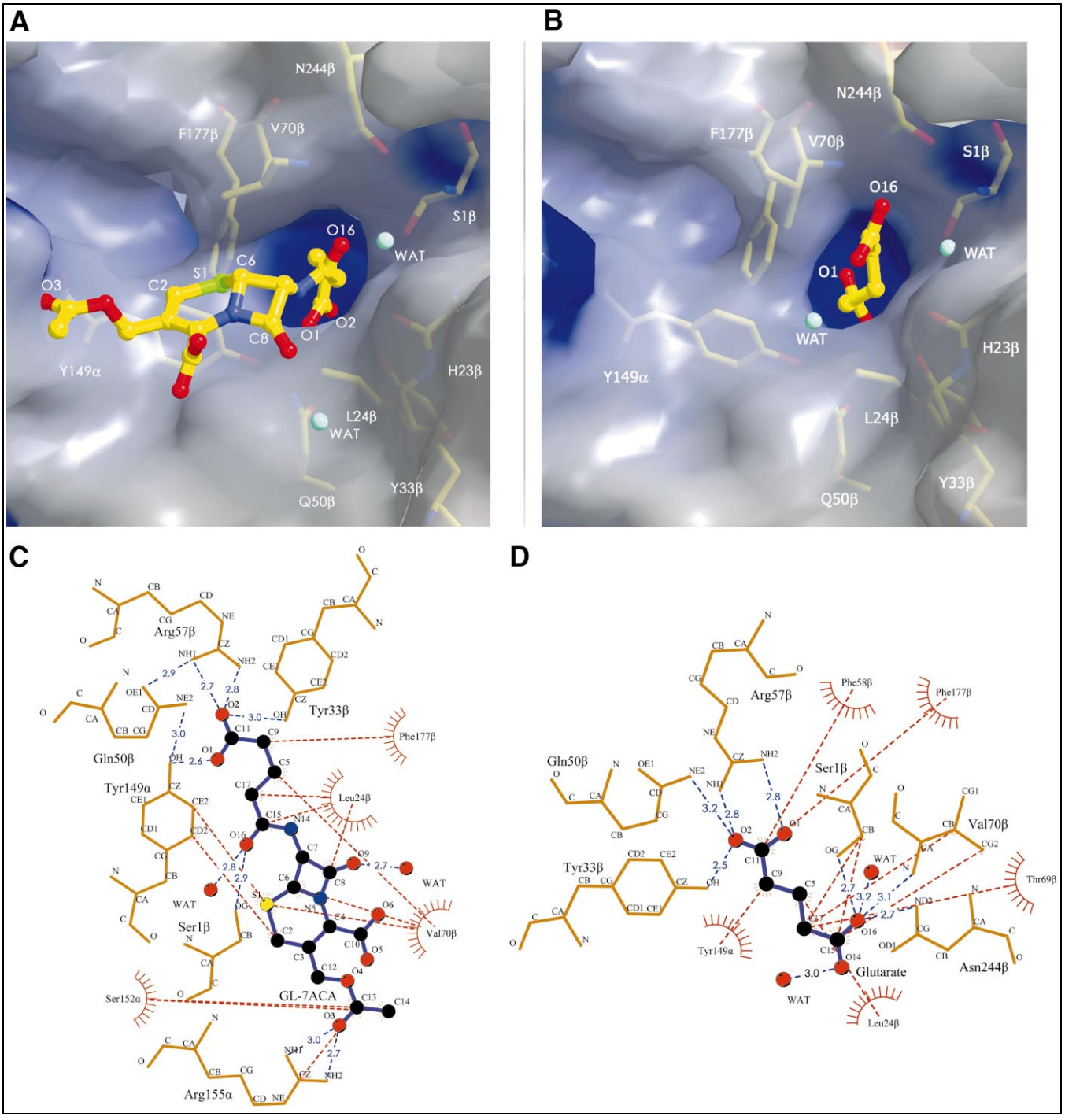


Fig. 2. Binding modes and interactions of ligands in active site. In the surface representation (A,B), blue and red correspond to positively and negatively charged areas, respectively. In (C) and (D) by LIGPLOT [37] the residues that make hydrogen bonds are in yellow stick models. The residues that make hydrophobic interactions are in red sunny side circles. Only the distances below 3.4 Å are indicated for hydrogen bonds (blue dashed lines). Hydrophobic interactions (red dashed lines) are indicated for distances below 3.9 Å. The ligands are in ball-and-stick models. The waters are labeled WAT. The carbon-to-nitrogen contacts are not depicted. (A) Surface presentation of active site with GL-7-ACA bound. The glutaryl moiety in the ball-and-stick model is buried deep in the positively charged side-chain binding pocket. The atoms S1, C2, C6, and C8 of GL-7-ACA (see also C) make hydrophobic interactions with protein, but the other atoms of the two rings are pointing solvent. The branched acetoxy chain makes hydrophilic and hydrophobic interactions with protein at the opposite end of the glutaryl moiety. (B) Surface presentation of active site with glutarate bound. The glutarate in the ball-and-stick model is buried in the side-chain binding pocket. The glutarate binds more out of the pocket towards the solvent, compared to the glutaryl moiety of GL-7-ACA (A). (C) Detailed interactions between GL-7-ACA and the residues of the active site in LIGPLOT. (D) Detailed interactions between glutarate and the residues of the side-chain pocket in LIGPLOT.

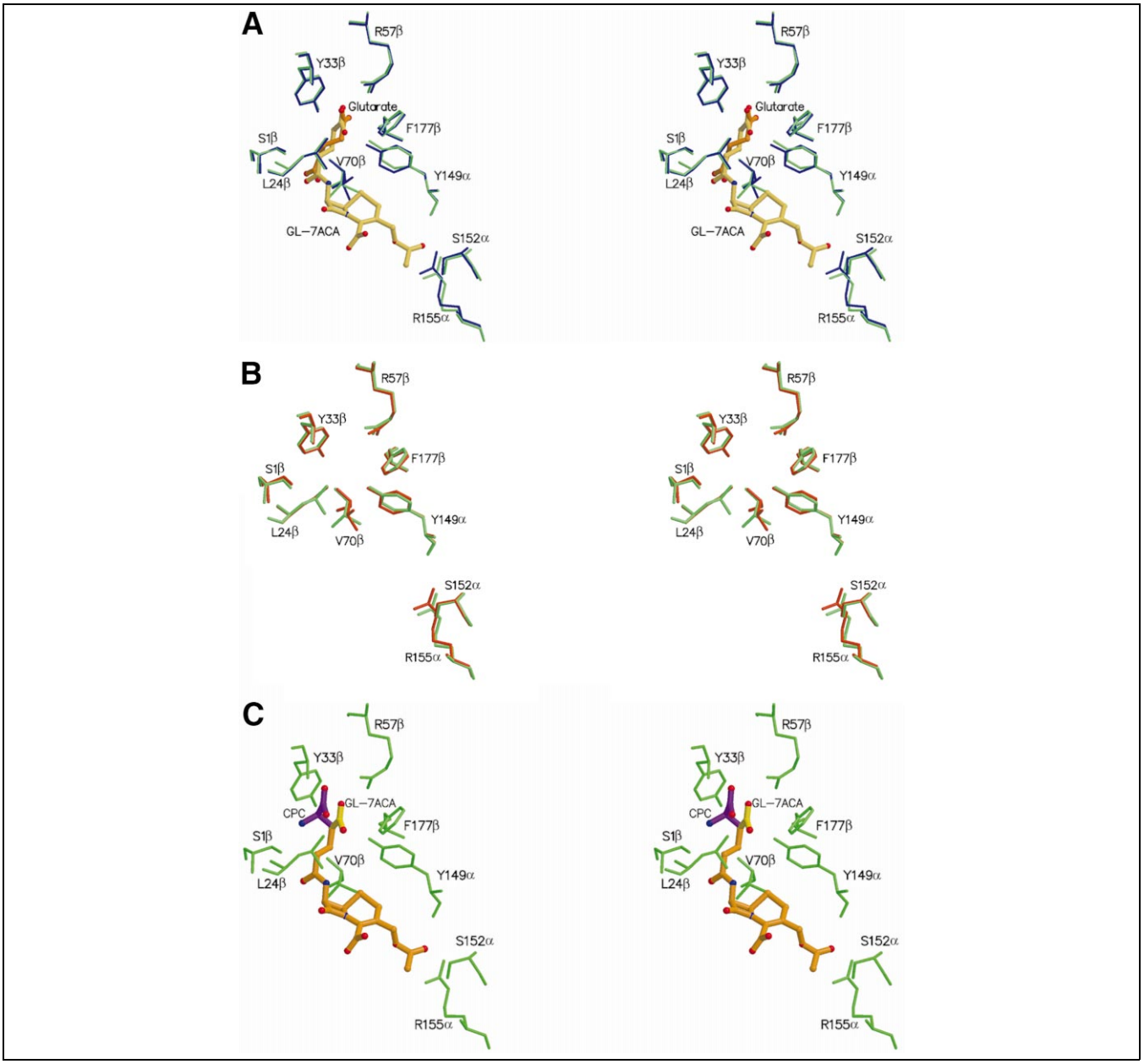


Fig. 3. Comparisons of ligand bound CAD structures. (A) A view of the overlaid positions of GL-7-ACA and glutarate. Nine interacting residues with GL-7-ACA in the GL-7-ACA bound structure (Fig. 2C) superimpose onto the corresponding residues of the glutarate bound structure in the stick models. The GL-7-ACA and glutarate are in yellow and orange, respectively, as shown in the ball-and-stick models. The residues of the GL-7-ACA bound structure are in green. The glutarate bound structure is in purple. (B) Superposition of the native and GL-7-ACA bound structures. Nine interacting residues with GL-7-ACA in the GL-7-ACA bound structure (Fig. 2C) are superimposed against the same residues of the native structure [12]. Active-site residues are shown in stick models. The residues of the GL-7-ACA bound structure are in green. The native structure is in red. (C) A model of CPC overlaid onto the refined GL-7-ACA structure with the nine interacting residues in the active site. GL-7-ACA is shown in orange except the carboxylate group in the side-chain binding pocket, which is in yellow. All of the atoms of CPC are modeled after the refined structure of GL-7-ACA, identical to that shown in orange. However, there is one additional carbon atom, and the amino group of the D-α-aminoadipyl moiety, compared to the glutaryl moiety of the GL-7-ACA, are extended to generate the D-α-aminoadipyl moiety (shown in purple). The carboxyl and amino groups of the D-α-aminoadipyl moiety (purple region) crash into the residues of the side-chain binding pocket (Arg57β, Tyr33β, Tyr149α) when they are rotated by torsional geometry.

the substrate, either in penicillin acylase or CA. A surface area of 606 Å$^2$ is buried while forming the glutarate:CAD complex, whereas only 100 Å$^2$ is buried while forming the four- and six-membered rings:CAD complex. Therefore, it seems that the specific hydrophilic and hydrophobic interactions, between the side-chain of the substrate and its binding pocket, are the dominating factors in recognizing the substrate in both CA (Fig. 2C,D) and penicillin acylase. Also, the binding energy, as a result of the hydrophobic interactions of the two fused rings with CAD,

might be offset by slightly less favorable interactions of the side-chain by itself, compared to the side-chain that is linked to the two fused rings.

### *2.4. Comparison of the binding patterns of GL-7-ACA and glutarate in side-chain pocket*

A comparison of the GL-7-ACA bound structure with the glutarate bound structure of CAD shows that the glutaryl moieties in these two structures do not exactly superimpose. The least square superposition (Fig. 3A) shows that the carbon atoms C9, C5, and C17 (Fig. 2C,D) of glutaryl moiety in the glutarate bound structure are displaced by 1.8, 1.4 and 1.2 Å, respectively, from the corresponding atoms of the GL-7-ACA bound structure. Yet, the most critical moiety, the carboxylate group, remains approximately in the same position forming hydrogen bonding interactions with Arg57β and Tyr33β (Fig. 2C,D). A small movement of the glutaryl moiety in the glutarate bound structure adjusts the interactions of glutarate with residues in the side-chain pocket, whose conformations are, in turn, slightly different from those in the GL-7-ACA, as shown in Fig. 3A. The root mean square (r.m.s) deviation for all of the 672 Cα atoms, between the GL-7-ACA bound structure and the glutarate bound structure, is 0.22 Å. Similarly, an r.m.s deviation of 0.18 Å, between the GL-7-ACA bound structure and the glutarate bound structure, is obtained by comparing the nine active-site residues that are involved in directly interacting with GL-7-ACA, as represented in Fig. 3A. The side-chain NE2 of Gln50β replaces a side-chain OH of Tyr149α in order to form a hydrogen bond with the oxygen of the glutarate. In addition, the patterns of hydrophobic interactions in the two complexes show a slight difference in that the four carbon atoms (C9, C5, C17, and C15 of the glutarate bound structure) form hydrophobic interactions to different residues from the ones of GL-7-ACA (shown in Fig. 2C,D). However, the overall interactions of each glutaryl moiety of the two structures are well conserved. This slightly different binding pattern, between the glutarate and GL-7-ACA bound structures, may be due to the fact that the glutaryl moiety of GL-7-ACA is confined to a certain conformation by the attached four-membered β-lactam ring, whereas a free glutarate can bind to the side-chain pocket to adopt a more favorable conformation without any constraint.

### *2.5. Few conformational changes between native and GL-7-ACA bound structures*

The superposition of the native CAD structure [12] and the GL-7-ACA bound structure of CAD reveals an r.m.s deviation of 0.23 Å for all 672 Cα atoms, and 0.22 Å for the nine active-site residues that interact with GL-7-ACA (Fig. 3B). Evidently, the binding of GL-7-ACA caused no noticeable conformational change in either the active site or the overall structure of the enzyme. The superposition of the glutarate bound structure onto the native structure shows a pattern similar to the GL-7-ACA bound CAD complex (data not shown). Hence, the GL-7-ACA complex of CAD appears to be an example of the so-called 'lock-and-key model' of substrate binding. The substrate 'key' is likely to adopt several major conformations in solution, one of which fits well into the 'lock' formed by the active-site of CAD. The glutarate side-chain of the GL-7-ACA bound to CAD causes no significant change in CAD (Fig. 3B). In this respect, the complex is similar to the phenylacetate (a side-chain of penicillin G, a substrate of PGA) that binds to PGA, which caused a small conformational change of the protein [29].

### *2.6. Model of CPC bound to the active site*

All CAs in the five classes of CA are able to convert several substrates and substrate analogs, but their activity on CPC varies from 0 to 4% relative to GL-7-ACA [8–12]. In the field of CA research, a key issue is how the enzymatic activity of the CAs can be increased with respect to CPC. As mentioned in the introduction, the improvement of CA activity for CPC, by both screening for a new CA and by protein engineering, has not yet made dramatic progress. The most active mutant CA from *Pseudomonas* N176 (N176) showed only one 15th of the activity for CPC compared to GL-7-ACA as a substrate [9,11]. For CAD, the most favored substrate is GL-7-ACA, but it showed no detectable activity versus CPC [16]. It would be interesting to examine which differences cause this dramatic change in activity between the glutaryl (side-chain of GL-7-ACA) and D-α-aminoadipyl moieties (side-chain of CPC).

To investigate this, a model of the D-α-aminoadipyl moiety of CPC was overlaid onto the refined structure of GL-7-ACA in complex with CAD. The backbone structure of CPC was kept the same as that of GL-7-ACA. An extra carbon atom and an amino group at the carboxyl end of side-chain of CPC were modeled in an extended conformation (Fig. 3C). This model of CPC bound to CAD shows that the carboxylate and amino groups of the D-α-aminoadipyl moiety in CPC would collide with critical active-site residues, such as Arg57β, Tyr33β and Tyr149α, which interact with the glutaryl moiety of GL-7-ACA in the side-chain pocket. Therefore, the direction of protein engineering to improve activity versus CPC should be to provide room to accommodate the extra carbon atom and amino group of CPC. This might be done by mutating bulky residues such as Arg57β, Tyr33β, Tyr149α, Phe177β and Gln50β into smaller ones with similar properties. For example, one might mutate Arg to Lys, Tyr to Thr, Gln to Asn and Phe to Val, or make combinatorial mutations for all four residues.

### 2.7. *Catalytic mechanism of the deacylation reaction of cephalosporin acylase*

In the GL-7-ACA complex with CAD (Fig. 4A), the target carbonyl carbon of GL-7-ACA is largely intact. Therefore, it is likely that the conformation of the bound GL-7-ACA closely resembles the Michaelis–Menten complex at the initial stage of the deacylation reaction. So far, a structure of a Michaelis–Menten complex has not been observed in either penicillin or CA. The catalytic nucleophile of CAD, OG of Ser1β, is positioned 3.4 Å away from the target carbonyl carbon C15 for the deacylation reaction. It is held in place by a 2.8 Å hydrogen bond with the main chain NH of His23β, while the Ntn amino group of Ser1β is held in place by the 2.8 Å hydrogen bond with the side-chain OD1 of Asn244β (Fig. 4A). The components for the oxyanion hole, as proposed in paper on the structure of penicillin acylase [28], are the main chain NH of Val70β (corresponding to Ala69β of PGA) and the side-chain ND2 of Asn244β (corresponding to Asn241β of PGA) in CAD. They are 3.9 Å and 4.5 Å away from the target carbonyl oxygen O16 (equivalent oxygen to oxyanion) of the GL-7-ACA, respectively (Fig. 4A). These distances are too long for hydrogen bonds to form, so the oxyanion hole cannot interact with the Michaelis–Menten complex.

In contrast to the GL-7-ACA bound to CAD, the negatively charged oxygen O16 of glutarate when bound to CAD, is stabilized by hydrogen bonds of the oxyanion hole (Fig. 4A). The distances of the O16 to the NH and the ND2 of the oxyanion hole are 3.1 Å and 2.6 Å, respectively. The equivalent oxygen O16 of GL-7-ACA in the GL-7-ACA:CAD complex is about 1 Å away from the oxygen O16 of the glutarate in the glutarate:CAD complex (Fig. 4A). The glutarate bound CAD structure seems to exhibit a binding pattern of a product–enzyme complex in which the oxyanion hole can interact with a negatively charged reaction product, glutarate.

The structure of a covalently inhibited penicillin acylase was determined at a 1.9 Å resolution by Duggleby et al.

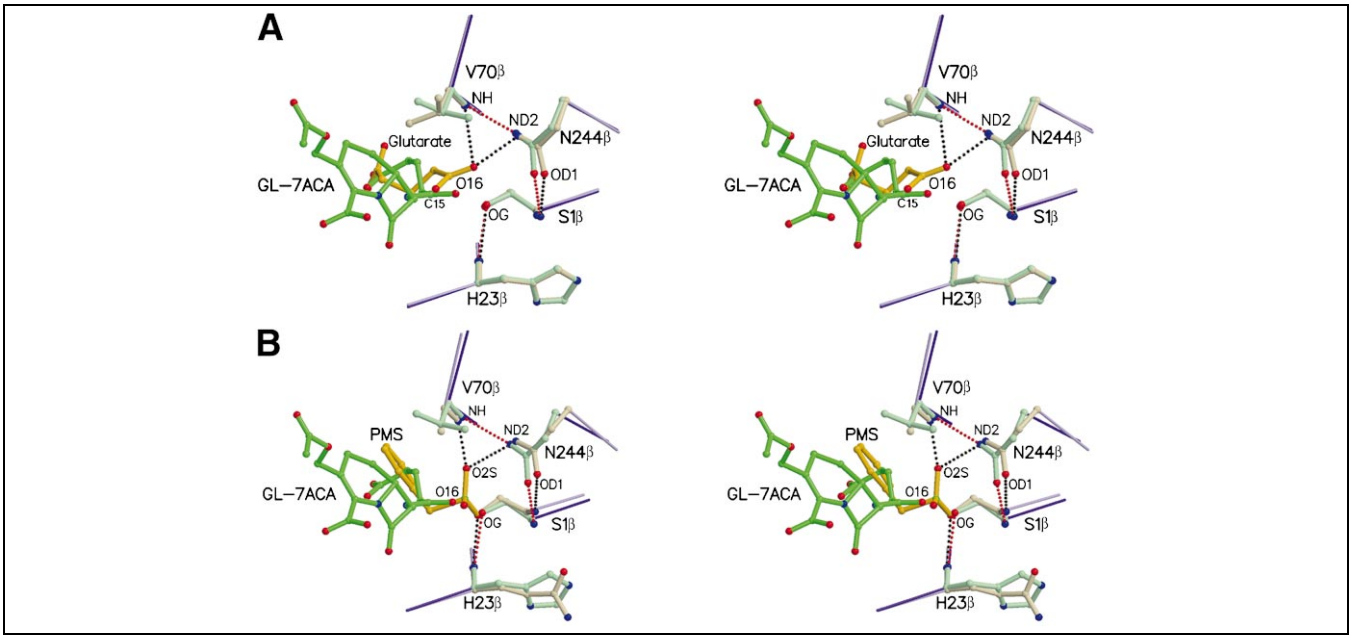


Fig. 4. Superposition of CAs and PGAs in complex with ligands with four catalytic residues. (A) Superposition of GL-7-ACA bound CAD onto glutarate bound CAD with four catalytic residues. Only the residues of the GL-7-ACA bound CAD (light green) are labeled: Ser1β, His23β, Val70β, and Asn244β of CAD in light green correspond to Ser1β, His23β, Val70β, and Asn244β of the glutarate bound CAD in light yellow, respectively. The Cα backbone of the GL-7-ACA bound CAD is colored purple. The light purple is for the Cα backbone of the glutarate bound CAD. The hydrogen bonds of the GL-7-ACA bound CAD are represented by red dash-lines. Black dash-lines are for the glutarate bound CAD. An oxyanion oxygen O16 of the glutarate (a product of the deacylation reaction from the side-chain of the substrate GL-7-ACA, colored in yellow) is stabilized by the two hydrogen bonds of the oxyanion hole that consists of the main chain NH of Val70β and the side-chain ND2 of Asn244β. However, the equivalent carbonyl oxygen O16 of the GL-7-ACA (colored in green) is 4.5 and 3.9 Å away from the corresponding atoms of the oxyanion hole. The label O16 represents the oxygen O16s from the two structures. (B) Superposition of GL-7-ACA bound CAD onto PMSF bound PGA with four catalytic residues [28]. Only the CAD residues are labeled as follows: Ser1β, His23β, Val70β, and Asn244β of CAD (light green) correspond to Ser1β, Asn23β, Ala69β, and Asn241β of PGA (light yellow), respectively. The Cα backbone of CAD is colored purple. Light purple is for the Cα backbone of PGA. The hydrogen bonds of CAD are represented by red dash-lines, and black dash-lines are for PGA. The GL-7-ACA bound CAD superimposes onto the PMSF bound PGA with an r.m.s. deviation of 0.38 Å in ten Cαs of the ten residues, including four catalytic residues. An oxyanion oxygen O2S of phenylmethane sulfonyl *O*-serine (transition state intermediate, labeled as PMS in yellow color) in the PGA structure is stabilized by two hydrogen bonds of the oxyanion hole that consists of the main chain NH of Ala69β and the side-chain ND2 of Asn241β. In contrast, the equivalent carbonyl oxygen O16 of the GL-7-ACA (colored in green) is 4.5 Å and 3.9 Å away from the putative oxyanion hole that consists of the main chain NH of Val70β and the side-chain ND2 of Asn244β, respectively.

[28]. Phenylmethylsulfonyl fluoride (PMSF) was covalently bound to Ser1β, which plays a key role in catalysis as a nucleophile. The tetrahedral geometry of the sulfonyl group may mimic the conformation of a transition state intermediate. The PMSF bound PGA structure, together with kinetic data, allowed a mechanism of the deacylation reaction for penicillin acylase to be proposed [28]. It was also proposed that CAD has a catalytic pathway analogous to that of PGA, since the active-site conformation of CAD is similar to PGA [12]. A transition state conformation is proposed in which the negatively charged carbonyl oxygen of the tetrahedral intermediate, generated by nucleophilic attack of the OG of Ser1β, is stabilized by hydrogen bonds from an oxyanion hole that consists of the main chain NH of Val70β (corresponding to Ala69β of PGA) and the side-chain ND2 of Asn244β (corresponding to Asn241β of PGA) (Fig. 4B). The Ntn amino group of Ser1β is also a crucial component in the chemical catalysis of the deacylation reaction. It is held in place by a water-mediated hydrogen bond with the nucleophile OG in the initial stage of the deacylation [28]. The oxyanion, oxygen O2S, of a suspected transition state intermediate, PMSF, in PGA is stabilized by the oxyanion hole.

Our two new binary complexes of CAD, together with the PMSF bound PGA structure of Duggleby et al. [28], give nearly a complete picture of the mode of substrate, transition state intermediate, and product binding to the active site of this important group of acylases during the deacylation reaction, as below. First, the substrate (GL-7-ACA) binds to the active site of the Michaelis–Menten complex, but the oxygen O16, corresponding to the transition state oxyanion, is about 1 Å away from the oxyanion hole (Fig. 4A,B). Second, the transition state intermediate (PMSF) is bound 1 Å closer to the oxyanion hole than the Michaelis–Menten complex, and is stabilized by hydrogen bonds with the oxyanion hole components (Fig. 4B). Third, the product (glutarate) remains bound to the active site in a similar conformation to the transition state intermediate (PMSF), where the oxygen O16 (corresponding to oxyanion) is stabilized by the oxyanion hole (Fig. 4A).

## 3. Significance

Semisynthetic cephalosporins are primarily synthesized from 7-ACA, which is obtained by the environmentally toxic chemical deacylation of CPC. Thus, the enzymatic conversion of CPC to 7-ACA by CA would be of great interest. CAs use GL-7-ACA as a primary substrate, and the enzyme has low turnover rates for CPC. The improvement of CA activity for CPC, by both screening for a new CA and by protein engineering, has not yet made dramatic progress. Attempts to obtain an enzymatic transformation of CPC into 7-ACA have led to the development of the two enzyme process using CA and D-amino acid oxidase.

Structures of the binary complexes of CA with GL-7-ACA, the most favored substrate of CAs, and glutarate, the side-chain of GL-7-ACA, reveal how the specific interactions in the active site cause GL-7-ACA to be the most favored substrate of a CA, and conversely explain why CPC is not a good substrate for a CA. The model of CPC bound to CA shows that the carboxylate and amino groups of the D-α-aminoadipyl moiety in CPC collides with critical active-site residues Arg57β, Tyr33β and Tyr149α. These substrate bound CAs will guide the direction of protein engineering to improve activity versus CPC towards a direct enzymatic transformation of CPC into 7-ACA by a single CA.

The catalytic mechanism of the deacylation reaction of CA was further elucidated by the two ligand bound structures: the substrate, GL-7-ACA, binds to the active site as the Michaelis–Menten complex and the product, glutarate, remains bound to the active site in a similar conformation to the transition state intermediate, where the oxygen O16 is stabilized by the oxyanion hole.

## 4. Materials and methods

### 4.1. Crystallization

CAD [15,16] was cloned into *Escherichia coli* BL21(DE3) with the overexpression vector pET24d(+). It was purified using phenyl Sepharose and Sephacryl-200 gel filtration column chromatography, as described elsewhere. The CAD concentration was 10 mg $ml^{-1}$ in a storage buffer (50 mM sodium phosphate, pH 7.0, and 150 mM NaCl). The 20 mM GL-7-ACA stock solution was prepared at pH 5.5, and the glutarate stock solution was in 200 mM concentration, pH 5.5. The ligand bound CAD crystals grew overnight at 21°C from hanging drops that contain 2 μl of the protein solution (10 mg $ml^{-1}$ CAD, 50 mM sodium phosphate, pH 7.0, and 150 mM NaCl), 1 μl of the 20 mM GL-7-ACA stock solution or 1 μl of the 200 mM glutarate stock solution, and 3 μl of the reservoir solution (20%(w/v) polyethylene glycol (PEG) 8000, 10 mM dithiothreitol (DTT), 200 mM magnesium acetate and 100 mM sodium cacodylate, pH 5.5) by the vapor diffusion method against a 500 μl reservoir solution. The ligand bound crystals grew under conditions similar to those of the native CAD crystals [12]. They belong to the same space group, $P4_12_12$, as the native CAD crystals and with almost identical unit cell dimensions. There is one αβ heterodimer of 77 kDa per asymmetric unit and the cell has a 57% solvent content. Crystals were transferred to a cryo-protectant solution that contained 23% (w/v) PEG 8000, 10%(w/v) glycerol, 200 mM magnesium acetate, 10 mM DTT, 100 mM sodium cacodylate, pH 5.5, 2.6 mM GL-7-ACA, or 26 mM glutarate (these ligand concentrations are a little lower than those used for crystallization) for 3 min before flash-cooling in a 100 K gaseous nitrogen stream.

### 4.2. Data collection

Data sets for the GL-7-ACA and glutarate bound crystals were collected at the Advanced Photon Source (APS) SBC-CAT beam-

line from frozen crystals. All data were indexed and integrated using DENZO and scaled by SCALEPACK [30].

### *4.3. Refinement*

The native CAD structure yielded an excellent initial crystallographic model for the ligand bound structures that needed only minor adjustments in the course of refinement. The $F_o-F_c$ difference Fourier maps provided an excellent guide for locating ligand locations (Fig. 1b–d). A glutaryl moiety, a carboxylate group and an acetoxymethyl moiety of the ligands were built using XtalView/Xfit [18] and O [19] onto a model structure of the four-membered β-lactam ring that was fused to a six-membered ring, obtained from the Cambridge Structural Database [20–22]. These models were used for the starting models for refinement cycles. All crystallographic refinements were carried out using CNS [23] with maximum-likelihood refinement. Model geometry was checked by PROCHECK [31]. The Ramachandran plot showed that 88.3%, 11%, and 0.5% of all residues for the glutarate bound structure are in the most favorable, the additionally allowed, and generously allowed regions, respectively. In the GL-7-ACA bound structure, 85.2%, 14.1%, and 0.5% are the most favorable, the additionally allowed, and generously allowed regions, respectively. Only one residue (Phe177β) in both structures, positioned in the active site, is located in a disallowed region. This agrees with the observation of Herzberg and Moult [32] that residues with unfavorable $\Phi,\Psi$ combinations tend to occur near functionally important residues of proteins. These aspects of the structures of CAD, complexed with GL-7-ACA and glutarate, are almost identical to the native structure. Data and refinement statistics are shown in Table 1. Figures are generated by MOLSCRIPT [33], BOBSCRIPT [34], RASTER3D [35], and GRASP [36].

### *4.4. Coordinates*

The coordinates are deposited in the Protein Data Bank with accession codes, 1JVZ (GL-7-ACA bound CA) and 1JW0 (glutarate bound CA).

## Acknowledgements

We thank Ethan Merritt, Stephen Suresh and Craig Behnke for their helpful discussions, Jungwoo Choe, Stewart Turley and Mic Feese for collecting data, and the SBC-CAT staff, in particular Randy Alkire, Stephan Ginell and Rongguang Zhang for their technical assistance on the APS SBC-CAT beamline. Use of the Argonne National Laboratory Structural Biology Center beamlines at the APS was supported by the US Department of Energy Office of Energy Research, under contract No. W-31-109-ENG-38. We also thank Francis Athappilly, Irwin Hirsh, and Claudia Roach of the Biomolecular Structure Center for maintaining our computer facilities and helping with the protein expression, purification and crystallization. W.G.J.H. acknowledges a major equipment grant from the Murdock Charitable Trust to the Biomolecular Structure Center. This study was supported by a Grant of the Korea Health 21 R&D Project, Ministry of Health and Welfare, Republic of Korea (01-PJ1-PG3-20900-0009) to Y.K.

## References

[1] IMS, Global pharmaceutical market growth accelerate to 7 percent in 1998, in: IMS Health Global services, Plymouth meeting, PA 19462-0905, 1998.
[2] F. Huber, B. Jackson, Preparative methods for 7-aminocephalosporanic acid and 6-aminopenicillanic acid in cephalosporins and penicillins, in: E. Flynn (Ed.), Chemistry and Biology, Academic press, New York, 1972, pp. 27–48.
[3] W. Tischer, F. Wedekind, Biocatalytic 7-aminocephalosporanic acid production, Ann. N. Y. Acad. Sci. 672 (1992) 502–509.
[4] G.J.M. Hersbach, P.W.M. Van Dijck, The penicillins: properties, biosynthesis and fermentation, in: E.J. Vandamme (Ed.), Biotechnology of Industrial Antibiotics, Marcel Dekker, New York, 1984, pp. 45–140.
[5] J. Velasco, J.L. Barredo, Environmentally safe production of 7-aminodeacetoxycephalosporanic acid (7-ADCA) using recombinant strains of *Acremonium chrysogenum*, Nat. Biotechnol. 18 (2000) 857–861.
[6] R. Binder, G. Romancik, Biochemical characterization of a glutaryl-7-aminocephalosporanic acid acylase from *Pseudomonas* strain BL072, Appl. Environ. Microbiol. 60 (1994) 1805–1809.
[7] A. Matsuda, K.I. Komatsu, Molecular cloning and structure of the gene for 7 beta-(4-carboxybutanamido)cephalosporanic acid acylase from a *Pseudomonas* strain, J. Bacteriol. 163 (1985) 1222–1228.
[8] I. Aramori, H. Imanaka, Comparative characterization of new glutaryl 7-ACA and cephalosporin C acylase, J. Ferment. Bioeng. 73 (1992) 185–192.
[9] Y. Ishii, K. Shimomura, High-level production, chemical modification and site-directed mutagenesis of a cephalosporin C acylase from *Pseudomonas* strain N176, Eur. J. Biochem. 230 (1995) 773–778.
[10] A. Matsuda, K. Komatsu, Cloning and characterization of the genes for two distinct cephalosporin acylases from a Pseudomonas strain, J. Bacteriol. 169 (1987) 5815–5820.
[11] Y. Saito, K. Shimomura, Oxidative modification of a cephalosporin C acylase from Pseudomonas strain N176 and site-directed mutagenesis of the gene, Appl. Environ. Microbiol. 62 (1996) 2919–2925.
[12] Y. Kim, W.J.G. Hol, The 2.0 Å crystal structure of cephalosporin acylase, Structure 8 (2000) 1059–1068.
[13] I. Aramori, H. Imanaka, Cloning and necleotide sequencing of new glutaryl 7-ACA and cephalosporin C acylase genes from *Pseudomonas* strains, J. Ferment. Bioeng. 72 (1991) 232–243.
[14] Y. Li, E. Wang, In vivo post-translational processing and subunit reconstitution of cephalosporin acylase from *Pseudomonas* sp. 130, Eur. J. Biochem. 262 (1999) 713–719.
[15] K.-H. Yoon, GenBank accession number AF251710, 1999.
[16] D.-W. Kim, K.-H. Yoon, Isolation of novel *Pseudomonas diminuta* KAC-1 strain producing glutaryl 7-aminocephalosporanic acid acylase, J. Microbiol. 37 (1999) 200–205.
[17] A.G. Murzin, C. Chothia, SCOP: a structural classification of proteins database for the investigation of sequences and structures, J. Mol. Biol. 247 (1995) 536–540.
[18] D. McRee, XtalView/Xfit: A versatile program for manipulating atomatic coordinates and electron density, J. Struct. Biol. 125 (1999) 156–165.
[19] T.A. Jones, Kjeldgaard, Improved methods for binding protein models in electron density maps and the location of errors in these models, Acta Crystallogr. A 47 (1991) 110–119.
[20] D.O. Spry, J.K. Swartzendruber, C(3)-azido cephem II, Tetrahedron Lett. 25 (1984) 2531–2534.

[21] G. Laurent, F. Durant, Preliminary results on the X-ray structure analysis of oxyimino cephalosporins, Eur. J. Med. Chem. 17 (1982) 281–284.
[22] A.P. Kuzin, J.R. Knox, Binding of cephalothin and cefotaxime to D-ala-D-ala-peptidase reveals a functional basis of a natural mutation in a low-affinity penicillin-binding protein and in extended-spectrum beta-lactamases, Biochemistry 34 (1995) 9532–9540.
[23] A.T. Brunger, G.L. Warren, Crystallography and NMR system: A new software suite for macromolecular structure determination, Acta Crystallogr. D Biol. Crystallogr. 54 (1998) 905–921.
[24] Y.S. Lee, S.S. Park, The role of α-amino group of the N-terminal serine of β-subunit for enzyme catalysis and autoproteolytic activation of glutaryl 7-aminocephalosporanic acid acylase, J. Biol. Chem. 275 (2000) 39200–39206.
[25] G.O. Daumy, F.J. Vinick, Experimental evolution of penicillin G acylases from *Escherichia coli* and *Proteus rettgeri*, J. Bacteriol. 163 (1985) 925–932.
[26] H.T. Huang, G.M. Shull, Distribution and substrate specificity of benzylpenicillin acylase, Appl. Microbiol. 11 (1963) 1–6.
[27] M.A. McDonough, J.A. Kelly, Crystal structure of penicillin G acylase from the Bro1 mutant strain of *Providencia rettgeri*, Protein Sci. 8 (1999) 1971–1981.
[28] H.J. Duggleby, P.C. Moody, Penicillin acylase has a single-amino-acid catalytic center, Nature 373 (1995) 264–268.
[29] S.H. Done, R.E. Hubbard, Ligand-induced conformational change in penicillin acylase, J. Mol. Biol. 284 (1998) 463–475.
[30] Z. Otwinowski, W. Minor, Processing of X-ray diffraction data collected in oscillation mode, Methods Enzymol. 276 (1997) 307–326.
[31] R.A. Laskowski, J.M. Thorton, PROCHECK – a program to check the stereochemical quality of protein structures, J. Appl. Crystallogr. 26 (1993) 283–291.
[32] O. Herzberg, J. Moult, Analysis of the steric strain in the polypeptide backbone of protein molecules, Proteins 11 (1991) 223–229.
[33] P.J. Kraulis, MOLSCRIPT: a program to produce both detailed and schematic plots of protein structures, J. Appl. Crystallogr. 24 (1991) 946–950.
[34] R.M. Esnouf, An extensively modified version of MolScript that includes greatly enhanced coloring capabilities, J. Mol. Graph. Model. 15 (1997) 132–134.
[35] E. Merritt, D.J. Bacon, Raster3D: photorealistic molecular graphics, Methods Enzymol. 277 (1997) 505–524.
[36] A. Nicholls, B. Honig, Protein folding and association: insights from the interfacial and thermodynamic properties of hydrocarbons, Proteins 11 (1991) 281–296.
[37] A.C. Wallace, J.M. Thornton, LIGPLOT: a program to generate schematic diagrams of protein–ligand interactions, Protein Eng. 8 (1995) 127–134.